⌘ *Author's Choice*

THE JOURNAL OF BIOLOGICAL CHEMISTRY VOL. 284, NO. 50, pp. 35092–35100, December 11, 2009
Printed in the U.S.A.

Structural Basis for the Role of the K65R Mutation in HIV-1 Reverse Transcriptase Polymerization, Excision Antagonism, and Tenofovir Resistance*[S]

Received for publication, May 20, 2009, and in revised form, September 24, 2009 Published, JBC Papers in Press, October 7, 2009, DOI 10.1074/jbc.M109.022525

Kalyan Das[‡§], Rajiv P. Bandwar[‡§], Kirsten L. White[¶], Joy Y. Feng[¶], Stefan G. Sarafianos[‡§1], Steven Tuske[‡§], Xiongying Tu[‡§], Arthur D. Clark, Jr.[‡§], Paul L. Boyer[‖], Xiaorong Hou[§], Barbara L. Gaffney[§], Roger A. Jones[§], Michael D. Miller[¶], Stephen H. Hughes[‖], and Eddy Arnold[‡§2]

From the [‡]Center for Advanced Biotechnology and Medicine (CABM) and the [§]Department of Chemistry and Chemical Biology, Rutgers University, Piscataway, New Jersey 08854, [¶]Gilead Sciences, Inc., Foster City, California 94404, and the [‖]HIV Drug Resistance Program, NCI-Frederick, National Institutes of Health, Frederick, Maryland 21702

K65R is a primary reverse transcriptase (RT) mutation selected in human immunodeficiency virus type 1-infected patients taking antiretroviral regimens containing tenofovir disoproxil fumarate or other nucleoside analog RT drugs. We determined the crystal structures of K65R mutant RT cross-linked to double-stranded DNA and in complexes with tenofovir diphosphate (TFV-DP) or dATP. The crystals permit substitution of TFV-DP with dATP at the dNTP-binding site. The guanidinium planes of the arginines K65R and Arg^{72} were stacked to form a molecular platform that restricts the conformational adaptability of both of the residues, which explains the negative effects of the K65R mutation on nucleotide incorporation and on excision. Furthermore, the guanidinium planes of K65R and Arg^{72} were stacked in two different rotameric conformations in TFV-DP- and dATP-bound structures that may help explain how K65R RT discriminates the drug from substrates. These K65R-mediated effects on RT structure and function help us to visualize the complex interaction with other key nucleotide RT drug resistance mutations, such as M184V, L74V, and thymidine analog resistance mutations.

During HIV-1 replication, the enzyme reverse transcriptase (RT)[3] converts the single-stranded viral genomic RNA into double-stranded DNA (dsDNA). Because of its essential role in the viral life cycle, RT is an important target for antiviral agents. Both nucleoside and nucleotide RT inhibitors (NRTIs) and non-nucleoside RT inhibitors are widely used as components of antiretroviral therapy for HIV-1 infection. The approved NRTIs are nucleoside or nucleotide analogs that are phosphorylated to their triphosphate or diphosphate active metabolites in cells (Fig. 1). NRTIs, once incorporated into the viral DNA, act as DNA chain terminators due to the lack of a 3′-OH group. RT with resistance mutations must maintain an adequate rate of nucleotide incorporation while recognizing dNTPs and enhancing discrimination against NRTIs or increasing the excision of incorporated NRTIs.

In HIV-1 RT, NRTI resistance mutations have a broad spatial distribution in and adjacent to the nucleotide substrate binding region (1). Different NRTI resistance mutations or sets of mutations are selected in response to treatment with different NRTIs. K65R emerges in response to treatment with tenofovir (TFV) disoproxil fumarate, abacavir, didanosine (ddI), or stavudine (2–4) and has recently been shown to have increased frequency in subtype C HIV-1 (5). Mutations M41L, D67N, K70R, L210W, T215F/Y, and K219Q/E/N (6), which are primary resistance mutations for AZT and stavudine, are called thymidine analog mutations (TAMs), AZT^r, or excision-enhancing mutations. TAMs cause cross-resistance to NRTIs by enhancing ATP-mediated excision (7–9) that we visualized in our recently determined crystal structures of RT·excision product complexes.[4] M184V/I is the primary mutation that causes resistance to lamivudine (3TC) and emtricitabine (10, 11). The Thr^{69} insertions occur in combination with TAMs and allow RT to excise a broader range of NRTIs (12–15). Q151M causes NRTI multidrug resistance that is often accompanied by several secondary mutations and termed the Q151M complex. There are complex interactions between these mutations that have a broad range of effects on NRTI resistance that drive their relative frequencies of occurring together. Among the most frequent in treatment-experienced populations are M184V and

* This work was supported, in whole or in part, by National Institutes of Health MERIT Award AI 27690 and Grant P01 GM 066671 (to E. A.) for support of RT structural studies and by the Intramural Research Program of the National Institutes of Health, NCI, Center for Cancer Research, and NIGMS (to S. H. H.).

⌘ *Author's Choice*—Final version full access.

The atomic coordinates and structure factors (codes 3JSM and 3JYT) have been deposited in the Protein Data Bank, Research Collaboratory for Structural Bioinformatics, Rutgers University, New Brunswick, NJ (http://www.rcsb.org/).

[S] The on-line version of this article (available at http://www.jbc.org) contains supplemental Figs. 1–5.

[1] Present address: Dept. of Molecular Microbiology and Immunology, Christopher S. Bond Life Sciences Center, University of Missouri, Columbia, MO 65211.

[2] To whom correspondence should be addressed: 679 Hoes Ln., Piscataway, NJ 08854. Tel.: 732-235-5323; Fax: 732-235-5289; E-mail: arnold@cabm.rutgers.edu.

[3] The abbreviations used are: RT, reverse transcriptase; AZT, zidovudine (3′-azido-2′,3′-deoxythymidine); 3TC, lamivudine (2′,3′-dideoxy-3′-thiacytidine); Bistris propane, 1,3-bis[tris(hydroxymethyl)methylamino]propane; 2AP-TP, 2-aminopurine analog of dATP; dsDNA, double-stranded DNA; NRTI, nucleotide and nucleoside RT inhibitor; HIV-1, human immunodeficiency virus, type 1; TFV, tenofovir; ddI, didanosine; TAM, thymidine analog mutation; DP, diphosphate; TP, triphosphate; ddATP, dideoxy-ATP; AZTppppA, AZT adenosine dinucleoside tetraphosphate; dATP-α-S, 2′-deoxyadenosine-5′-*O*-(1-thiotriphosphate).

[4] X. Tu, K. Das, J. D. Bauman, Q. Han, A. D. Clark, X. Hou, Y. V. Frenkel, B. L. Gaffney, R. A. Jones, P. L. Boyer, S. H. Hughes, S. G. Sarafianos, and E. Arnold, unpublished data.

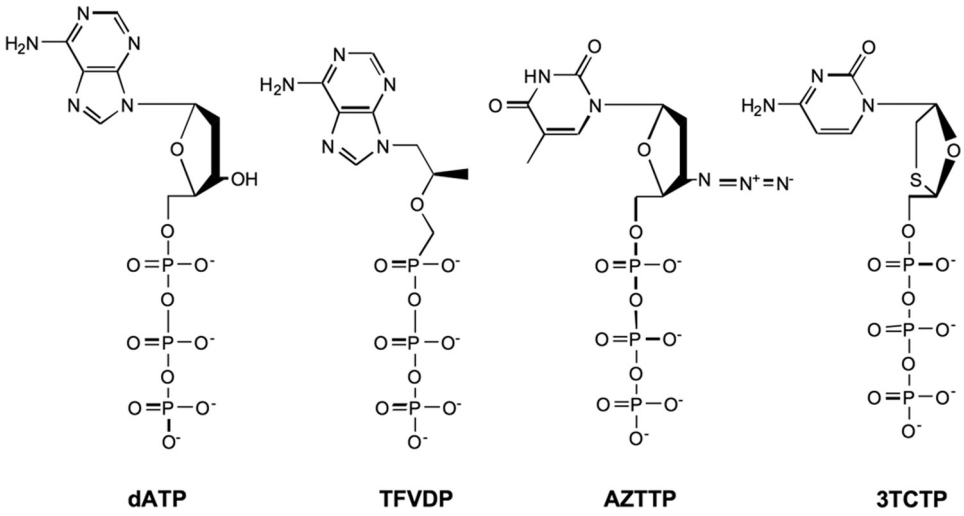

FIGURE 1. **Chemical structures of dATP, TFV-DP, AZT-TP, and 3TC-TP.**

TAMs, and less frequent but positively associated are M184V with K65R (16–18); in contrast, K65R and TAMs or K65R and L74V are rarely present together (19, 20).

TFV, administered as the prodrug TFV disoproxil fumarate, is among the most widely prescribed antiretroviral drug in the United States and Europe. K65R causes reduced susceptibility to TFV disoproxil fumarate and all other NRTIs with the exception of AZT. K65R results in a virus with reduced fitness that is attributed to a slower rate of incorporation (k_{pol}) for the natural dNTP substrates (21). K65R is further able to discriminate against all NRTIs by having an even slower incorporation rate than the natural substrates (22–25). Interestingly, K65R also has a reduced rate of excision of NRTIs that is most pronounced for AZT and results in a counteraction of the incorporation and excision resistance mechanisms that restores full AZT susceptibility (26, 27). The most relevant crystal structures available for analyzing K65R are of wild-type HIV-1 RT·dsDNA in complexes with dTTP (28) or TFV-DP (29). These structures provide the basic framework for understanding DNA polymerization and binding of TFV-DP to RT, but they do not explain the effects of the K65R mutation on polymerization, excision, or TFV resistance. Several modeling studies have proposed that the K65R mutation alters the positioning and binding of the NRTI-TP or surrounding amino acid residues or that the conformational mobility of the K65R-containing fingers loop is reduced (21, 24, 30–32), however, there is no universal agreement on the structural basis for the broad effects of the K65R mutation. Here we report the crystal structures of ternary complexes of K65R mutant RT·dsDNA with TFV-DP or the natural substrate dATP. The K65R crystal structures presented here show how this mutation restricts the structural adaptability of the enzyme by forming a molecular platform involving the conserved residue Arg^{72}; the platform may discriminate against the incorporation of NRTIs, interfere with the binding of ATP as an excision substrate, and interact with other NRTI resistance mutations.

EXPERIMENTAL PROCEDURES

Expression, Purification, and Crystallization of RT—K65R HIV-1 RT was expressed in *Escherichia coli* and purified, as reported earlier (29). The K65R mutation is present on the p66 subunit only, which also contains a mutation Q258C for cross-linking with the nucleic acid. The p51 subunit is truncated at the C terminus residue 428, followed by Gly-Gly-His_7. The mutation C280S is present in both subunits. A 27-mer template DNA (5′-ATG GTC GGC GCC CGA ACA GGG ACT GTG-3′) was custom synthesized by Integrated DNA Technologies (Coralville, IA). The 20-mer primer DNA (5′-ACA GTC CCT GTT CGG **G**CG CC-3′) bearing a cross-linkable thioalkyl tether (on **G** in the sequence) was synthesized and annealed to the template. The 27:20-mer dsDNA was cross-linked to K65R RT at the p66 C258 site, the cross-linked primer was extended with a dideoxy-G at the 3′-end through RT polymerization (33), the cross-linked K65R RT·dsDNA complex was purified using Ni^{2+}-nitrilotriacetic acid and heparin columns in tandem, and the purified complex was concentrated to ~10 mg/ml. The K65R RT·dsDNA sample was co-crystallized with TFV-DP by hanging drop vapor diffusion against the well solution containing 50 mM Bistris propane, pH 6.4, 100 mM ammonium sulfate, 5% (v/v) glycerol, 5% (w/v) sucrose, 10% (w/v) polyethylene glycol 8000, and 20 mM $MgCl_2$ (or $MnCl_2$). The crystallization drops, containing 2 μl of RT·dsDNA·TFV-DP added to 2 μl of the well solution, produced crystals in 2–3 weeks at 4 °C. Crystals of K65R RT·dsDNA·dATP were obtained by soaking the crystals of K65R RT·dsDNA·TFV-DP in the well solution containing 10 mM dATP for 10 min. The substitution of TFV-DP by dATP in the crystal by soaking was confirmed using a fluorescent dATP analog (supplemental Fig. 1).

Crystallography—Crystals of K65R RT·dsDNA·TFV-DP complex were stabilized in crystallization buffer containing 12% polyethylene glycol 8000 and then cryoprotected by dipping in the respective transfer solution containing 25% glycerol for ~5 s and cryocooled in liquid N_2. The x-ray diffraction data sets were collected at Cornell High Energy Synchrotron Source beam line F1. Three different data sets, each to 3 Å resolution, were collected from three crystals of K65R RT·dsDNA·TFV-DP; two crystals grew in the presence of $MgCl_2$, and one grew in the presence of $MnCl_2$. The structure was solved by molecular replacement using the protein atoms from the wild-type RT·dsDNA·TFV-DP structure (29) as the starting model. The model was refined using the three individual data sets that were non-isomorphous. The crystallographic phases and figures of merit from individually refined structures were input to DMMULTI in CCP4 (34) for multiple crystal form averaging that improved the phases and reduced model bias. The difference electron density ($|F_o| - |F_c|$) maps were strong and clear for TFV-DP (Fig. 2*A*), the model for which was not included in the initial stages of refinement. Cycles of model building and refinement using one of the three data sets yielded the final structure of K65R RT·dsDNA·TFV-DP (Table 1). Binding of

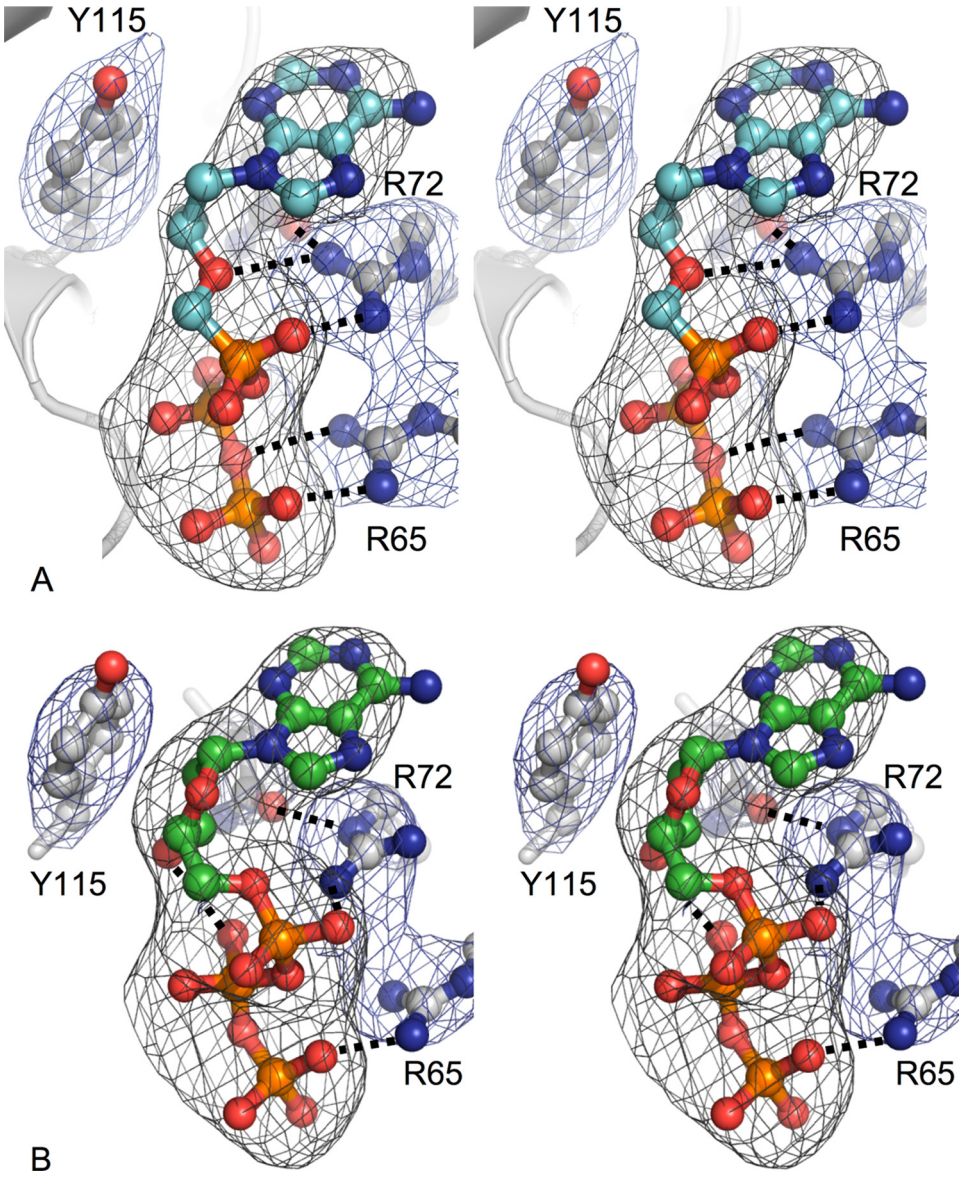

FIGURE 2. **Binding of TFV-DP and dATP to K65R RT.** *A*, stereoview showing the binding of TFV-DP (*cyan/orange*) to K65R mutant RT (*gray*) in the K65R RT·dsDNA·TFV-DP ternary complex structure. The sections of difference ($|F_o| - |F_c|$) electron density maps were calculated at 3.0 Å resolution and contoured at 3.5σ (3.0 electrons/Å^3) for TFV-DP and 2.2σ (1.4 electrons/Å^3) for the interacting amino acid residues. The hydrogen bond interactions are represented by *dotted lines*. *B*, stereoview showing the binding of dATP (*green/orange*) to K65R mutant RT (*gray*) in the K65R RT·dsDNA·dATP ternary complex structure. The sections of difference ($|F_o| - |F_c|$) electron density maps were calculated at 3.3 Å resolution and contoured at 3.5σ (3.1 electrons/Å^3) for dATP and 2.0σ (1.4 electrons/Å^3) for the RT residues. For both structures, the maps covering the substrate/inhibitor were calculated prior to their inclusion into refinement cycles. The electron density for the β3-β4 region was substantially improved after inclusion of the substrate/inhibitor in structure refinements. Therefore, the difference maps covering the protein side chains were calculated after omitting the residues and refining the structures to remove model bias.

one metal at the polymerase active site in the current structures was confirmed by the electron density map calculated from the crystal that contained $MnCl_2$ during crystallization (supplemental Fig. 3).

The K65R RT·dsDNA·dATP complex was obtained by soaking the crystals of K65R RT·dsDNA·TFV-DP in crystallization solution containing 10 mM dATP for 10 min. The soaked crystals were stabilized at 12% polyethylene glycol 8000 and cryoprotected following the procedure described for TFV-DP-containing crystals. The 10 mM concentration of dATP was maintained in both the stabilization and cryoprotectant solutions. The dATP-soaked crystals were very sensitive to x-ray exposure; therefore, diffraction data from three crystals were merged to obtain an almost complete data set (Table 1) with high redundancy. High redundancy (~13.5) of data resulted in a relatively high R_{merge} value; however, the merged overall data set produced better quality electron density maps compared with the maps from less complete individual data sets. The K65R RT·dsDNA model from the K65R RT·dsDNA·TFV-DP structure was used to determine the structure of the K65R RT·dsDNA·dATP complex. Programs CNS 1.2 (35) and COOT (36) were used for refining and model building of both of the structures. The diffraction data and refinement statistics are listed in Table 1. The coordinates and structure factors for the crystal structures of K65R mutant RT·dsDNA·TFV-DP and K65R mutant RT·dsDNA·dATP complexes are available from the Protein Data Bank with accession codes 3JSM and 3JYT, respectively.

Pre-steady State Kinetics of Single Nucleotide Incorporation—For the biochemical studies, wild-type and K65R mutant heterodimeric p66/p51 HIV-1 RT were expressed and purified as described (27). The DNA 19-mer primer (5′-GTCCCTGTTCGGGCGCCAC) and 36-mer template D36A (5′-TCTCTATGTGTGGCGCCCGAACAGGGACCTGAAAGC) were used in the study. Pre-steady state constants (k_{pol}) were determined using dATP (Roche Applied Science) or dATP-α-S (Sp isomer) (Biolog, Bremen, Germany) at 5 times the K_d value (200 μM for wild-type RT and 75 μM for K65R RT) and 100 nM active wild-type or K65R RT with a KinTek rapid quench-flow apparatus as described (37).

RESULTS

Ternary Complex of K65R Mutant RT·dsDNA·TFV-DP—The crystal structure of K65R RT·27:21-mer dsDNA·TFV-DP (supplemental Fig. 2) was determined at 3.0 Å resolution and refined to R_{work} and R_{free} of 0.252 and 0.285, respectively, using 49,494 reflections (Table 1). Multiple crystal form averaging

TABLE 1
Diffraction data and refinement statistics

	K65R mutant RT·dsDNA·TFV-DP	K65R mutant RT·dsDNA·dATP
Protein Data Bank code	3JSM	3JYT
X-ray source	CHESS F1	CHESS F1
No. of crystals used	1	3
Wavelength (Å)	0.9179	0.9179
Space group	$P3_112$	$P3_112$
Cell constants (a, b, c in Å; α, β, γ in degrees)	170.31, 170.31, 155.44; 90, 90, 120	169.72, 169.72, 155.41; 90, 90, 120
Resolution range (Å)	50.0–3.0	50–3.3
No. of unique reflections (no. of observations)	49,494 (164,942)	37,809 (510,405)
Completeness (%)	95.9	98.6
R_{merge} [a] (in last shell)	0.156 (0.563)	0.190 (0.724)
R_{meas} [b]	0.184 (0.708)	0.177 (0.611)
Average $I/\sigma(I)$	5.6	8.6
σ cut-off	−1.0	−1.0
Refinement statistics		
Total no. of atoms (DNA/inhibitor or substrate atoms)	8,855 (901/27)	8,853 (901/30)
Resolution (Å)	50.0–3.0	50–3.3
No. of reflections (R_{free} set)	49,494 (1,530)	37,789 (1,140)
Completeness (%)	95.8	98.5
Cut-off criteria	$\|F\| \leq 0$	$\|F\| \leq 0$
R_{work}	0.252	0.253
R_{free}	0.285	0.287
Root mean square deviations		
Bond lengths (Å)	0.009	0.008
Bond angles (degrees)	1.69	1.46

[a] $R_{merge} = \Sigma_{hkl} \Sigma_i |I(hkl)_i - \langle I(hkl)\rangle| / \Sigma_{hkl} \Sigma_i \langle I(hkl)_i\rangle$.
[b] $R_{meas} = \Sigma_h [m/(m-1)]^{<sfrax,1,2>} \Sigma_i |I_{h,I} - \langle I_h\rangle| / \Sigma_h \Sigma_i I_{h,I}$, where m represents the multiplicity of each reflection, Σ_h is taken over all unique reflections, and Σ_i is taken over the set of independent observations of each unique reflection.

using three independent data sets yielded improved and unbiased electron density maps that helped to enhance the quality of this structure. The ternary complex of K65R RT crystallized in a crystal form similar to that of wild-type RT·dsDNA·TFV-DP (29). Comparison of the wild type and K65R mutant structures shows similar RT conformation, mode of dsDNA-binding, and crystal packing; the root mean square deviation for all Cα atoms is ~0.5 Å when both structures are overlaid. The position and conformation of TFV-DP in the new structure could be determined by well defined electron density in difference maps calculated prior to the inclusion of the TFV-DP molecule in the refinement (Fig. 2*A*). The TFV-DP molecule in the structure unambiguously fits the electron density in a low energy conformation, base-pairs with the first template overhang, and coordinates a catalytic Mg^{2+} ion via three phosphate oxygen atoms. As observed in the wild-type RT·dsDNA·TFV-DP crystal structure, only one Mg^{2+} ion (metal-B) is present in the polymerase active site that coordinates with the catalytic aspartates Asp^{110} and Asp^{185}, the main-chain carbonyl of Val^{111}, and one oxygen atom from each phosphate group of TFV-DP. The presence of only one metal ion at the active site of the current structure was confirmed by determining the crystal structure of K65R RT·dsDNA·TFV-DP with Mn^{2+} ions (supplemental Fig. 3) replacing Mg^{2+} ions, which is in agreement with our earlier analysis (38) indicating that the binding of the second Mg^{2+} ion at the polymerase active site requires coordination with Asp^{186}. In the current structures, the side chain of D186 has turned away from the putative metal-A binding site.

Amino acid residues K65R, Arg^{72}, and Tyr^{115}, which interact with TFV-DP, are clearly defined in the electron density map (Fig. 2), and key interactions of RT with the bound nucleotide substrate are maintained. The mutated residue K65R has an orientation similar to Lys^{65} in the wild-type RT·dsDNA·TFV-DP (29) and wild-type RT·dsDNA·dTTP structures (28) where one of the guanidinium Nη nitrogens interacts with the γ-phosphate oxygen (N . . . O distance of 2.6 Å). The other guanidinium Nη nitrogen of K65R interacts with the oxygen atom linking the β- and γ-phosphates of TFV-DP, which mimics the interaction of K65 with TFV-DP in the wild-type RT·dsDNA·TFV-DP structure (29).

The major difference between wild-type and the K65R RT structures is at the $\beta3$-$\beta4$ fingers loop. The Cα position of Arg^{65} on the flexible $\beta3$-$\beta4$ loop is displaced ("pushed back") by about the length of a covalent bond (~1.5 Å) compared with the Cα position of Lys^{65} in the dTTP-bound wild-type RT structure for accommodating 1-bond length longer arginine when substituted for lysine (supplemental Fig. 3). The rearrangement of the $\beta3$-$\beta4$ loop accommodates a sulfate ion that interacts with the side chain of Arg^{72} and the main chain amide group of Lys^{66}. The guanidinium plane of K65R is stacked with the guanidinium plane of Arg^{72} with an approximate distance of 3.8 Å between the two guanidinium planes. The Arg^{72} guanidinium plane is also stacked on its other side with the adenine base of TFV-DP. Arg^{72} is a highly conserved amino acid residue that is critical for RT function. The side chain of Arg^{72} interacts with all three components (base, sugar, and α-phosphate) of an incoming dNTP (Fig. 2) and is expected to stabilize the transition state of the nucleophilic attack by the 3′-end of the primer on the α-phosphate of the dNTP. A comparison of the crystal structures of the RT ternary complexes suggests that the stacking of the guanidinium groups of K65R and the conserved Arg^{72} imposes a constraint on adaptability of both of the amino acid residues. To obtain a better understanding of how the K65R mutation helps RT discriminate between TFV-DP and dATP, we also determined the crystal structure of the K65R mutant RT·dsDNA·dATP complex.

Ternary Complex of K65R Mutant RT·dsDNA·dATP—Our attempt to co-crystallize dATP with the 27:21-mer dsDNA cross-linked K65R mutant RT produced crystals that had a shape similar to the rodlike crystals of K65R RT·dsDNA·

TFV-DP complex; however, the crystals of the dATP complex did not grow to a size suitable for diffraction studies. Therefore, the feasibility of exchanging the incoming nucleotides was evaluated. Crystals of the RT·dsDNA·TFV-DP complex were soaked with 5 mM 2AP-TP for 5 min, and fluorescence of 2-aminopurine was measured. The resulting fluorescence demonstrated that 2AP-TP had replaced TFV-DP (supplemental Fig. 1). This approach was used to obtain the structure of the RT·dsDNA·dATP complex by soaking the natural substrate dATP into the crystals of RT·dsDNA·TFV-DP complex. The soaked crystals diffracted X-rays to 3.3 Å compared with the 3.0 Å resolution diffraction from the parent RT·dsDNA·TFV-DP crystals. The dATP-soaked crystals were relatively sensitive to radiation damage, and diffraction data from three crystals were merged to obtain the final data set. The structure solution revealed clear electron density for the dATP molecule and the interacting amino acid residues (Fig. 2*B*). The final model was refined to R_{work} and R_{free} of 0.253 and 0.287, respectively, using a total of 37,789 reflections (Table 1).

The overall structure of K65R RT·dsDNA·dATP complex is similar to that of K65R RT·dsDNA·TFV-DP complex. The adenine bases and the triphosphates of TFV-DP and dATP superimpose when the two ternary complex structures of K65R mutant RT are compared (Fig. 3*A*). TFV-DP has an acyclic phosphonomethoxypropyl group substituted for the ribose α-phosphate moiety of dATP (Fig. 1); this difference can be seen in the superimposed structures. In the dATP-bound structure, the ribose ring is stacked against the aromatic ring of Tyr^{115}. The 3′-OH of dATP forms a hydrogen bond network with its β-phosphate oxygen (3.1 Å) and the main-chain amino group of Tyr^{115} (distance 3.1 Å). Because TFV-DP lacks a 3′-OH group, the interactions that involve the 3′-OH of dATP are not present, and the methyl group of TFV-DP stacks with Tyr^{115} in a way that is analogous to but less extensive than the stacking of the ribose ring of dATP and Tyr^{115}. Superposition of the two structures shows that the oxygen atom in the phosphonomethoxypropyl group of TFV-DP is positioned ~1.7 Å away from the ribose C4* atom of dATP (Fig. 3*A*), which reorients the side-chain rotameric conformation of Arg^{72}. In the TFV-DP-bound K65R RT structure, Arg^{72} has a rotameric conformation (rotamer-2) that is analogous to the orientation of Arg^{72} in the wild-type RT·dsDNA·TFV-DP structure (29) but distinct from a common R72 rotamer (rotamer-1) in dATP-, dTTP- (28), and AZTppppA-bound RT·dsDNA structures[4]; the two distinct rotameric conformations of Arg^{72} differ by ~1.6 Å at the position of Nϵ (Fig. 3); the distinct rotameric conformations of Arg^{72} in TFV-DP *versus* dATP-bound RT ternary complexes were further confirmed by our recent high resolution structures of RT·RNA-DNA·TFV-DP (or dATP) complexes determined at 2.57 (or 2.6) Å.[5] The rotamer-2 conformation of Arg^{72} allows both Nη atoms to have polar interactions with TFV-DP, whereas only one Nη atom of Arg^{72} (in the rotamer-1 conformation) can have such interactions with dATP. This difference in these interactions might partly compensate for the complete loss of the 3′-OH hydrogen-bonding network and partial loss of stacking with Tyr^{115} for TFV-DP compared with dATP. The side chain of K65R also has two rotameric conformations, depending on whether dATP or TFV-DP is bound (Fig. 3, *B* and *C*). These different rotamers facilitate better stacking of the guanidinium planes of K65R and Arg^{72} in the two structures.

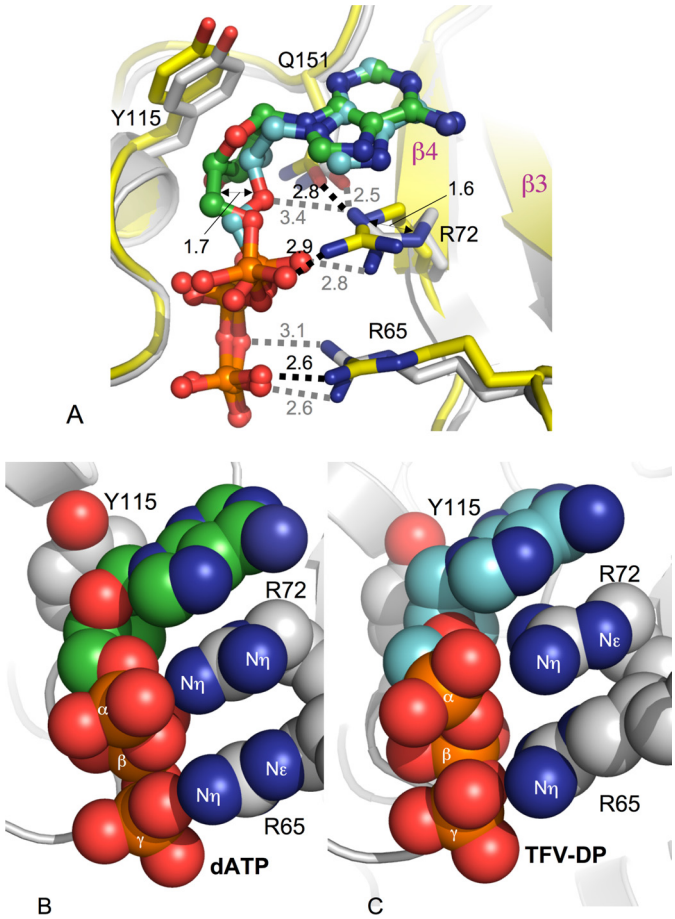

FIGURE 3. **Comparison of binding of TFV-DP and dATP to K65R RT·dsDNA.** *A*, overlay of TFV-DP (TFV-DP (*cyan*) and RT (*gray*)) and dATP (dATP (*green*) with RT (*yellow*)) shows that the structural difference between the inhibitor and the substrate at the deoxyribose moiety positions Arg^{72} and Arg^{65} side chains differently. The polar interactions are represented by *dotted lines*. Shown is stacking of the guanidinium plane of Arg^{65} and guanidinium plane of Arg^{72} and adenine base in K65R RT·dsDNA·dATP (*B*) and K65R RT·dsDNA·TFV-DP (*C*) ternary structures. Despite differences in the rotameric conformations of Arg^{65} and Arg^{72}, the hydrophobic stacking is maintained in both structures.

Incorporation Kinetics of dNTP and NRTIs—Biochemical studies showed that the K65R mutation can cause drug resistance to NRTIs and reduce both the nucleotide incorporation and excision by RT. Three independent pre-steady state analyses of K65R incorporation of dATP *versus* the NRTIs TFV-DP and ddATP (the active metabolite of ddI) are summarized in Table 2 (23, 25, 39). In all studies, the K65R mutant shows a modest decrease in the incorporation rate (k_{pol}) for dATP (4.5-fold) without a significant change in the binding affinity (K_d). K65R RT is resistant to TFV-DP and ddATP because the mutation dramatically decreases the incorporation of these analogs (>20-fold).

The kinetic steps of dNTP incorporation (k_{pol}) for HIV-1 RT consist of the conformational step of the closing down of the fingers loop ($\beta3$-$\beta4$) that contains residue 65 that leads to the

[5] K. Das, R. P. Bandwar, J. D. Bauman, and E. Arnold, unpublished data.

TABLE 2
Summary of relative pre-steady state kinetic constants

Substrate	Change of wild type *versus* K65R[a]		
	k_{pol}[b]	K_d[c]	k_{pol}/K_d[d]
		-fold	
dATP	4.5	2.1	2.1
TFV-DP	28.7	1.5	19.1
ddATP	23.3	0.9	25.9

[a] The average of the measured kinetic constants from two to three independent studies of WT and K65R RT were tabulated, and the -fold changes are shown (23, 25, 39).
[b] The -fold change of the average k_{pol} is shown, where increased -fold change in k_{pol} is representative of a decreased rate of substrate incorporation for K65R *versus* wild type.
[c] The -fold change of the average K_d is shown, where increased -fold change in K_d is representative of the decreased K_d and increased substrate binding affinity for K65R *versus* wild type.
[d] The -fold change of the average k_{pol}/K_d, where increased -fold change in k_{pol}/K_d is representative of decreased incorporation efficiency of K65R *versus* wild type.

TABLE 3
Steady state kinetic constants for incorporation of dATP and dATP-α-S

RT	Incorporation rate (k_{pol})[a] dATP	dATP-α-S	Elemental effect[b]
		s^{-1}	
Wild type	70 ± 3	70 ± 2	1.0
K65R	16.5 ± 0.6	14.3 ± 0.2	1.1

[a] The average of the measured kinetic constants from two independent measurements using wild-type and K65R RT.
[b] The phosphorothioate elemental effect is defined as $k_{pol}^{dATP}/k_{pol}^{dATP\text{-}\alpha\text{-}S}$.

positioning of dNTP for nucleophilic attack and the chemical step of phosphodiester bond formation (40–43). Evidence for the conformational change of the fingers loop as the rate-limiting step during polymerization *versus* the chemistry step has been generated by studying the incorporation of modified dNTPs that contain a phosphorothioate group at the α-phosphate (dNTP-α-S). The difference in the rate of incorporation of a natural dNTP and the dNTP-α-S is termed the "elemental effect" (44). The rate of the chemical step is estimated to be decreased 30–100-fold by the presence of the thio group; thus, an elemental effect close to 1 suggests that the incorporation rate (k_{pol}) is determined primarily by a rate-limiting step other than the chemistry step. The elemental effect for wild-type and K65R RT was investigated (Table 3). K65R showed a comparably slower k_{pol} for incorporation of dATP and dATP-α-S by 4.2- and 4.9-fold, respectively. Thus, the elemental effect observed for wild-type and K65R mutant HIV-1 RT was 1.0 and 1.1, respectively (Table 3), supporting the hypothesis that the K65R mutation slows the rate-limiting conformational step for nucleotide incorporation, probably by conformational restriction by the K65R/Arg^{72} molecular platform rather than the chemical step of incorporation.

DISCUSSION

Significance of the K65R Mutation for RT Function—Biochemical and clinical data have shown that K65R has broad phenotypic effects on NRTIs. Clinically, the K65R resistance mutation develops after treatment with abacavir, ddI, stavudine, and TFV disoproxil fumarate and causes reduced susceptibility to all approved NRTIs with the exception of AZT, where full susceptibility is retained (20). Biochemically, K65R RT decreases the rate of incorporation (k_{pol}) of all natural substrates and approved NRTI drugs; the incorporation kinetics of the adenosine analogs dATP, TFV-DP, and ddATP (the active metabolite of ddI) determined by several groups are shown in Table 2. An α-boranophosphate-modified ddATP, however, incorporates slightly more efficiently than dATP for K65R RT (45). Interestingly, any other substitution at position 65 also significantly decreases both the binding and the incorporation of dNTPs and catalytic efficiency of polymerization (31, 46). The rate of reverse reaction of pyrophosphorolysis and ATP-mediated excision is also decreased. This is most notable for incorporated AZT, where the decreased incorporation of AZT-TP is counteracted by significantly decreased excision after its incorporation that results in full susceptibility of K65R viruses to this NRTI (14, 26, 27).

Previous crystal structures of wild-type HIV-1 RT ternary complexes show interaction between the Nζ atom of Lys^{65} and the γ-phosphate of the dNTP. In the current K65R structures, one of the guanidinium nitrogens of Arg^{65} functionally replaces the Nζ atom of Lys^{65} by interacting with a γ-phosphate/β-γ-linker oxygen of dNTP (or TFV-DP) (*i.e.* in general, the mutation does not alter the hydrogen-bonding interactions of the bound dNTP (or an analog)). In fact, the bound dATP has only one polar interaction with Arg^{65}, and the interaction is analogous to the interaction between dTTP and Lys^{65} (28). The K65R substitution adds a bulky guanidinium group, which can form additional hydrogen bonds with restricted geometry (47) and can participate in hydrophobic stacking. The guanidinium groups of Arg^{65} and Arg^{72} are stacked in both K65R mutant structures (Fig. 3, *B* and *C*); the Arg^{72} guanidinium plane is also stacked with the adenine base of dATP (or TFV-DP). Two guanidinium nitrogens of Arg^{72} form hydrogen bonds with the α-phosphate (or phosphonate) of the dNTP (or TFV-DP) and the side chain of Gln^{151}. Residue Arg^{72} would be required to adapt to subtle changes in dNTP conformation in the steps of binding, incorporation, or excision. As is evident from the current structures, the K65R mutation restricts the adaptability of both the Arg^{65} and Arg^{72} side chains via the stacking of guanidinium planes. In fact, Arg^{65} and Arg^{72} stack to form a stable platform that interacts with all three parts (base, deoxyribose/acyclic linker, and α-phosphates/phosphonate) of dATP or TFV-DP (Fig. 3), which might explain the reduced rate of nucleotide incorporation by K65R mutant RT compared with wild-type RT (Table 2). The structural constraint by the K65R/Arg^{72} platform may also act like a "checkpoint" that helps discriminate among dNTPs for correct base pairing with the template, which thereby provides a possible explanation for the reported increase in fidelity of the K65R mutant (30). The lack of a significant elemental effect suggests that the mutation primarily affects the conformational change rather than the phosphodiester bond formation (Table 3). These kinetic data correlate with the structural information indicating that the K65R/Arg^{72} platform would restrain the movements of these residues and hinder the efficiency of nucleotide incorporation/excision. The decreased rates of the incorporation of dNTPs appear to account for decreased viral replication capacity of the K65R mutant (30).

K65R Mutation and Resistance to TFV—The major chemical difference between TFV-DP and dATP is the substitution of an

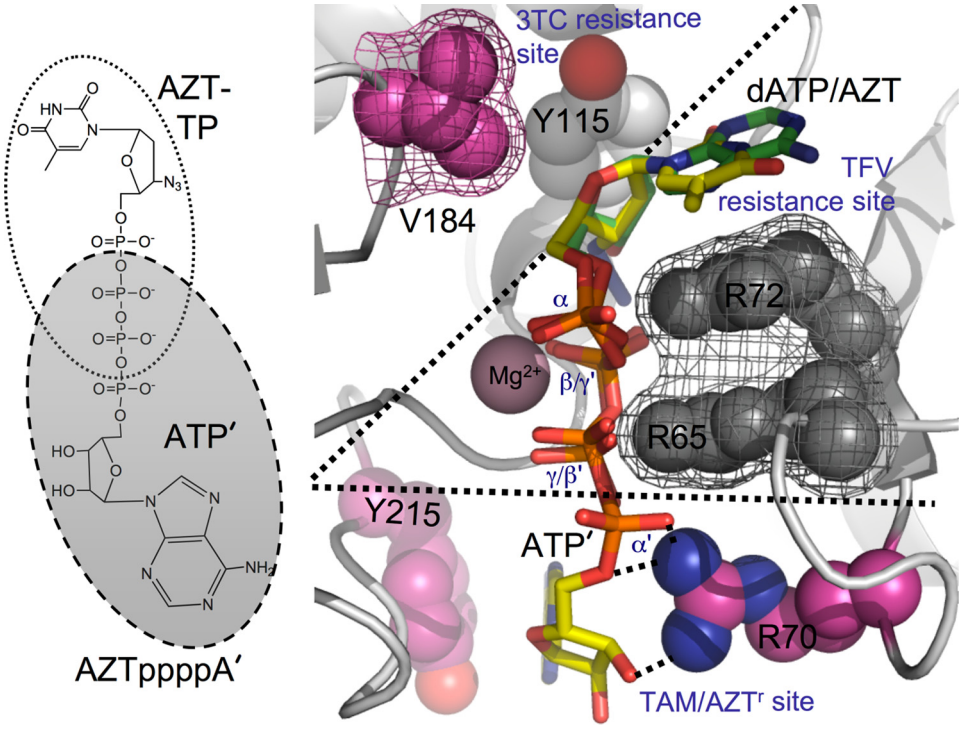

FIGURE 4. **Three distinct mechanisms of NRTI resistance through mutations at three distinct sites.** Superposition of excision-enhancing mutation or TAM (M41L, D67N, K70R, T215Y, and K219Q) RT·dsDNA·AZTppppA structure[4] on K65R RT·dsDNA·dATP structure at their dNTP-binding sites; AZTppppA is the product of AZT monophosphate by ATP-mediated excision. Although the two structures contained two distinct sites of mutations and crystallized in two distinct space groups, they superimpose very well at the active site region. The mutated residues Arg^{70} and Tyr^{215} are from the crystal structure of excision-enhancing mutation RT complex, whereas M184V was modeled based on the structure of the M184V RT·dsDNA binary complex (49). The surfaces of the K65R/Arg^{72} platform (*gray mesh*) and M184V (3TC resistance mutation site; *magenta mesh*) form two walls on either side of the ribose ring, whereas the other end of the K65R/Arg^{72} platform interfaces with K70R, a primary mutation site for AZT resistance.

acyclic phosphonomethoxypropyl group for the deoxyribose α-phosphate moiety of dATP (Fig. 1). In the crystal structures, these distinct chemical moieties of TFV-DP and dATP also have different structural arrangements, whereas the remaining parts of dATP and TFV-DP superimpose (Fig. 3*A*). As discussed above, this structural difference results in Arg^{72} having a rotamer-2 conformation in both the wild-type (29) and K65R mutant RT ternary complexes with TFV-DP compared with the common rotamer-1 conformation in the structures of the K65R RT·dsDNA·dATP, wild-type RT·dsDNA·dTTP (28), wild-type RT·dsDNA·AZTppppA, and TAM RT·dsDNA·AZTppppA complexes,[4] all of which have superimposable deoxyribose rings. The rotamer-1 and rotamer-2 conformations of Arg^{72} both facilitate the hydrophobic stacking with the adenine base of dATP (or TFV DP) and maintain key polar interactions with the α-phosphate/phosphonate and Gln^{151} but through different sets of atoms (Fig. 3) (*e.g.* an Nη atom of Arg^{72} is hydrogen-bonded with Gln^{151} in the TFV-DP-bound structure compared with the Nϵ atom of Arg^{72} in the dATP-bound structure). Additionally, the Nη atom has a weaker polar interaction with the phosphonomethoxypropyl oxygen of TFV-DP; an Nη atom can donate two hydrogens compared with the Nϵ atom, which donates only one. All oxygen atoms (from $P_{\alpha'}$, phosphonomethoxypropyl moiety, and Gln^{151}) that interact with the Nη/Nϵ atom are almost co-planar with the Arg^{72} guanidinium plane (Fig. 3), consistent with the geometrical restriction imposed by a planar guanidinium group (47). Several pre-steady state kinetic studies (summarized in Table 2) for dATP, TFV-DP, and ddATP show that the preferential modes of binding of the K65R/Arg^{72} platform to TFV-DP do not improve or disfavor its binding affinity compared with the natural substrate dATP. In fact, for all substrates characterized by pre-steady state kinetics, the binding affinity of K65R is minimally affected compared with wild-type RT (23, 25, 39).

The alternate conformation of Arg^{72} (rotamer-2) permits the guanidinium group to interact with the phosphonomethoxypropyl oxygen while stacking with the adenine ring of TFV-DP and guanidinium plane of Arg^{65}. The locked alternate conformation of Arg^{72} imposed by the K65R mutation in the TFV-DP-bound structure may further restrict Arg^{72} to attain conformations or an electronic configuration that might be required for the catalytic steps of the polymerization reaction. Our structural results are consistent with biochemical and clinical findings, and the structural analyses further suggest that the K65R mutation discriminates TFV-DP from dATP by locking Arg^{72} in an alternate conformation (rotamer-2) when TFV-DP is bound. This constraint on Arg^{72} is relaxed in wild-type RT, where Lys^{65} cannot engage in guanidinium stacking with Arg^{72}. The K65R mutation has a more significant effect on incorporation of ddATP than on the incorporation of dATP (Table 2), although the only difference between the two is that ddATP lacks the 3′-OH. As seen in the dATP-bound K65R RT structure (Fig. 2*B*), the 3′-OH helps define the relative positioning of the deoxyribose and the phosphates through its interaction with the β-phosphate oxygen and the main-chain amino group of Tyr^{115}. The loss of the interactions with the 3′-OH might also account for the observation that ddATP is incorporated more slowly by wild-type RT than is dATP. The absence of this interaction network, added to the constraint imposed by the K65R/Arg^{72} platform, may prevent ddATP from attaining the positioning of the phosphates and the dideoxyribose ring required for optimal incorporation.

Implications for K65R Interactions with Other Resistance Mutations—K65R is surrounded by other residues associated with NRTI resistance and is commonly associated with M184V or Q151M but is negatively associated with others, such as L74V or most TAMs (20). The K65R/M184V double mutant has increased resistance to the NRTIs ddI, abacavir, 3TC, and emtricitabine but improved susceptibility to TFV, stavudine, and AZT compared with K65R alone (23, 48). The mutations

K65R and M184V impose structural restraints on the two sides of the deoxyribose binding site (supplemental Fig. 4) to cause reduced incorporation efficiency of natural nucleotides (23). The M184V-mediated positional constraints and narrowing at the polymerase active site are consistent with the observed increase in K_d for dNTP binding (49). The incorporation of TFV-DP, which has a flexible acyclic oxypropyl linker substituted for the ribose ring, is minimally affected by the addition of the β-branched M184V mutation and K65R-induced platform (Fig. 4 and supplemental Fig. 4), whereas the natural substrate dATP is more affected by the smaller and less adaptable binding pocket.

Mutations that are negatively associated with K65R show unfavorable complementarity with the K65R/Arg^{72} platform. L74V is negatively associated with K65R (20, 50) and is positioned underneath the template base that complements the base of the incoming dNTP (supplemental Fig. 5). Leu^{74} is surrounded by the side chains of Phe^{61}, Ile^{63}, Arg^{72}, and Gln^{151}, which provide it a compact hydrophobic environment to support the template base that is analogous to the Arg^{72} support of the base of the incoming dNTP. Both residues appear critical for maintaining the base pairing between the dNTP and the template. Our modeling (supplemental Fig. 5) suggests that the constraint on Arg^{72} caused by the K65R mutation (via the K65R/Arg^{72} platform) and the alteration of the adjacent molecular surface by the L74V mutation removes the support for the template base proximal to where it is base-paired with the dNTP (supplemental Fig. 5), causing drastically reduced substrate incorporation kinetics (21).

TAMs (M41L, D67N, K70R, T215Y/F, and K219Q/E/N) cause enhanced NRTI excision, a major mechanism of resistance where the excision of incorporated nucleotides is mediated by ATP. Our recent crystal structure of a TAM RT bound to primer-template and AZTppppA (the ATP-mediated excision product of AZT monophosphate; Fig. 4) has shown that T215Y significantly contributes to the binding of ATP to the mutant RT for excision by stacking with its adenine base and K70R forms a network of hydrogen-bonding interactions with the α′-phosphate and 3′-OH of ATP.[4] The K65R mutation has the opposite effect of decreasing the rate of excision due in part to the K65R/Arg^{72} platform-based conformational constraints (Fig. 4) (27, 51, 52). The comparison of the interactions of K70R and K65R shows that the two residues interact with ATP, and the positioning of K70R would be affected by the K65R mutation and vice versa. It is likely that the guanidinium groups of K70R and K65R may stack together and extend the K65R/Arg^{72} platform to Arg^{72}/K65R/K70R if RT contains both a K65R and a K70R mutation. This extended platform would add further constraints that may not support adequate RT function and may explain the antagonistic relationship between the K65R and K70R mutations (26, 53). T215Y is located further away from K65R mutation site; however, the K65R/Arg^{72} platform is likely to interfere with the positioning of β′- and γ′-phosphates of ATP and constrain the conformational mobility of the fingers loop, thus decreasing the efficiency of excision (24, 26). Given these types of incompatibilities among NRTI mutations, these structural results help to explain the clinical benefit of administering TFV disoproxil fumarate with other widely used NRTI drugs AZT and 3TC, where the development of resistance to all NRTIs either occurs rarely or occurs with a fitness cost to the virus.

CONCLUSIONS

Discrimination between a nucleotide analog and a natural nucleotide can occur at the steps of binding to RT, catalytic reaction of polymerization, and/or enhanced excision. Different mutations (or sets of mutations) generate resistance to NRTIs through distinct mechanisms. Biochemical and structural data have elucidated two distinct mechanisms of NRTI resistance of 1) discrimination due to steric hindrance by M184V/I mutation to 3TC-TP and emtricitabine-TP (49, 54) and 2) the ATP-mediated excision of incorporated NRTIs exemplified by the TAMs (7–9), which is the primary mechanism of resistance to AZT. Our current structures demonstrate a third "conformational restriction" mechanism of NRTI resistance that cross-talks with the previous two NRTI resistance mechanisms. The K65R mutation neither enhances nor reduces the interaction of dATP or TFV-DP in the precatalytic complexes with RT; rather, the side chain of K65R has an enhanced interaction with the side chain of Arg^{72} to form a molecular platform that restricts adaptability of the polymerase active site and causes both a decreased rate of substrate incorporation and NRTI excision (23, 25). The effect of K65R appears to be on the rate-limiting conformational step of nucleotide incorporation; this idea is supported by the lack of an elemental effect that would also affect the excision reaction. An analogous platform with alternate rotameric conformations for both Arg^{72} and Arg^{65} is created upon binding of TFV-DP that enhances the ability of RT to discriminate between TFV-DP and dATP.

Acknowledgments—We acknowledge the personnel at the Cornell High Energy Synchrotron Source for data collection and the members of our laboratories for valuable conversations and assistance. We also thank Ann Stock for spectrophotometer access and Joe Bauman, Hans Reiser, James Chen, Mary McGrath, S. Swaminathan, Damian McColl, and Margaret Benton for helpful discussion.

REFERENCES

1. Arnold, E., Das, K., Ding, J., Yadav, P. N., Hsiou, Y., Boyer, P. L., and Hughes, S. H. (1996) *Drug Des. Discov.* **13,** 29–47
2. Winters, M. A., Shafer, R. W., Jellinger, R. A., Mamtora, G., Gingeras, T., and Merigan, T. C. (1997) *Antimicrob. Agents Chemother.* **41,** 757–762
3. Harrigan, P. R., Stone, C., Griffin, P., Nájera, I., Bloor, S., Kemp, S., Tisdale, M., and Larder, B. (2000) *J. Infect. Dis.* **181,** 912–920
4. Margot, N. A., Lu, B., Cheng, A., and Miller, M. D. (2006) *HIV Med.* **7,** 442–450
5. Coutsinos, D., Invernizzi, C. F., Xu, H., Moisi, D., Oliveira, M., Brenner, B. G., and Wainberg, M. A. (2009) *J. Virol.* **83,** 2029–2033
6. Larder, B. A., and Kemp, S. D. (1989) *Science* **246,** 1155–1158
7. Meyer, P. R., Matsuura, S. E., So, A. G., and Scott, W. A. (1998) *Proc. Natl. Acad. Sci. U.S.A.* **95,** 13471–13476
8. Meyer, P. R., Matsuura, S. E., Mian, A. M., So, A. G., and Scott, W. A. (1999) *Mol. Cell* **4,** 35–43
9. Boyer, P. L., Sarafianos, S. G., Arnold, E., and Hughes, S. H. (2001) *J. Virol.* **75,** 4832–4842
10. Tisdale, M., Kemp, S. D., Parry, N. R., and Larder, B. A. (1993) *Proc. Natl. Acad. Sci. U.S.A.* **90,** 5653–5656

11. Faraj, A., Agrofoglio, L. A., Wakefield, J. K., McPherson, S., Morrow, C. D., Gosselin, G., Mathe, C., Imbach, J. L., Schinazi, R. F., and Sommadossi, J. P. (1994) *Antimicrob. Agents Chemother.* **38,** 2300–2305
12. Mas, A., Parera, M., Briones, C., Soriano, V., Martínez, M. A., Domingo, E., and Menéndez-Arias, L. (2000) *EMBO J.* **19,** 5752–5761
13. Boyer, P. L., Sarafianos, S. G., Arnold, E., and Hughes, S. H. (2002) *J. Virol.* **76,** 9143–9151
14. Meyer, P. R., Lennerstrand, J., Matsuura, S. E., Larder, B. A., and Scott, W. A. (2003) *J. Virol.* **77,** 3871–3877
15. White, K. L., Chen, J. M., Margot, N. A., Wrin, T., Petropoulos, C. J., Naeger, L. K., Swaminathan, S., and Miller, M. D. (2004) *Antimicrob. Agents Chemother.* **48,** 992–1003
16. Catucci, M., Venturi, G., Romano, L., Riccio, M. L., De Milito, A., Valensin, P. E., and Zazzi, M. (1999) *J. Acquir. Immune Defic. Syndr.* **21,** 203–208
17. Masquelier, B., Descamps, D., Carrière, I., Ferchal, F., Collin, G., Denayrolles, M., Ruffault, A., Chanzy, B., Izopet, J., Buffet-Janvresse, C., Schmitt, M. P., Race, E., Fleury, H. J., Aboulker, J. P., Yeni, P., and Brun-Vézinet, F. (1999) *Antivir. Ther.* **4,** 69–77
18. Whitcomb, J. M., Parkin, N. T., Chappey, C., Hellmann, N. S., and Petropoulos, C. J. (2003) *J. Infect. Dis.* **188,** 992–1000
19. Parikh, U. M., Bacheler, L., Koontz, D., and Mellors, J. W. (2006) *J. Virol.* **80,** 4971–4977
20. McColl, D. J., Chappey, C., Parkin, N. T., and Miller, M. D. (2008) *Antiviral Ther.* **13,** 189–197
21. Deval, J., Navarro, J. M., Selmi, B., Courcambeck, J., Boretto, J., Halfon, P., Garrido-Urbani, S., Sire, J., and Canard, B. (2004) *J. Biol. Chem.* **279,** 25489–25496
22. Gu, Z., Arts, E. J., Parniak, M. A., and Wainberg, M. A. (1995) *Proc. Natl. Acad. Sci. U.S.A.* **92,** 2760–2764
23. Deval, J., White, K. L., Miller, M. D., Parkin, N. T., Courcambeck, J., Halfon, P., Selmi, B., Boretto, J., and Canard, B. (2004) *J. Biol. Chem.* **279,** 509–516
24. White, K. L., Chen, J. M., Feng, J. Y., Margot, N. A., Ly, J. K., Ray, A. S., Macarthur, H. L., McDermott, M. J., Swaminathan, S., and Miller, M. D. (2006) *Antivir. Ther.* **11,** 155–163
25. Sluis-Cremer, N., Sheen, C. W., Zelina, S., Torres, P. S., Parikh, U. M., and Mellors, J. W. (2007) *Antimicrob. Agents Chemother.* **51,** 48–53
26. Parikh, U. M., Zelina, S., Sluis-Cremer, N., and Mellors, J. W. (2007) *AIDS* **21,** 1405–1414
27. White, K. L., Margot, N. A., Ly, J. K., Chen, J. M., Ray, A. S., Pavelko, M., Wang, R., McDermott, M., Swaminathan, S., and Miller, M. D. (2005) *AIDS* **19,** 1751–1760
28. Huang, H., Chopra, R., Verdine, G. L., and Harrison, S. C. (1998) *Science* **282,** 1669–1675
29. Tuske, S., Sarafianos, S. G., Clark, A. D., Jr., Ding, J., Naeger, L. K., White, K. L., Miller, M. D., Gibbs, C. S., Boyer, P. L., Clark, P., Wang, G., Gaffney, B. L., Jones, R. A., Jerina, D. M., Hughes, S. H., and Arnold, E. (2004) *Nat. Struct. Mol. Biol.* **11,** 469–474
30. Shah, F. S., Curr, K. A., Hamburgh, M. E., Parniak, M., Mitsuya, H., Arnez, J. G., and Prasad, V. R. (2000) *J. Biol. Chem.* **275,** 27037–27044
31. Sluis-Cremer, N., Arion, D., Kaushik, N., Lim, H., and Parniak, M. A. (2000) *Biochem. J.* **348,** 77–82
32. Kagan, R. M., Lee, T. S., Ross, L., Lloyd, R. M., Jr., Lewinski, M. A., and Potts, S. J. (2007) *Antiviral Res.* **75,** 210–218
33. Sarafianos, S. G., Clark, A. D., Jr., Tuske, S., Squire, C. J., Das, K., Sheng, D., Ilankumaran, P., Ramesha, A. R., Kroth, H., Sayer, J. M., Jerina, D. M., Boyer, P. L., Hughes, S. H., and Arnold, E. (2003) *J. Biol. Chem.* **278,** 16280–16288
34. Potterton, E., McNicholas, S., Krissinel, E., Cowtan, K., and Noble, M. (2002) *Acta Crystallogr. D Biol. Crystallogr.* **58,** 1955–1957
35. Brunger, A. T. (2007) *Nat. Protoc.* **2,** 2728–2733
36. Emsley, P., and Cowtan, K. (2004) *Acta Crystallogr. D Biol. Crystallogr.* **60,** 2126–2132
37. Feng, J. Y., Shi, J., Schinazi, R. F., and Anderson, K. S. (1999) *FASEB J.* **13,** 1511–1517
38. Das, K., Sarafianos, S. G., Clark, A. D., Jr., Boyer, P. L., Hughes, S. H., and Arnold, E. (2007) *J. Mol. Biol.* **365,** 77–89
39. Svarovskaia, E. S., Feng, J. Y., Margot, N. A., Myrick, F., Goodman, D., Ly, J. K., White, K. L., Kutty, N., Wang, R., Borroto-Esoda, K., and Miller, M. D. (2008) *J. Acquir. Immune Defic. Syndr.* **48,** 428–436
40. Kati, W. M., Johnson, K. A., Jerva, L. F., and Anderson, K. S. (1992) *J. Biol. Chem.* **267,** 25988–25997
41. Reardon, J. E. (1992) *Biochemistry* **31,** 4473–4479
42. Hsieh, J. C., Zinnen, S., and Modrich, P. (1993) *J. Biol. Chem.* **268,** 24607–24613
43. Radzio, J., and Sluis-Cremer, N. (2005) *Protein Sci.* **14,** 1929–1933
44. Mizrahi, V., Henrie, R. N., Marlier, J. F., Johnson, K. A., and Benkovic, S. J. (1985) *Biochemistry* **24,** 4010–4018
45. Selmi, B., Boretto, J., Sarfati, S. R., Guerreiro, C., and Canard, B. (2001) *J. Biol. Chem.* **276,** 48466–48472
46. Garforth, S. J., Kim, T. W., Parniak, M. A., Kool, E. T., and Prasad, V. R. (2007) *J. Mol. Biol.* **365,** 38–49
47. Mason, P. E., Neilson, G. W., Dempsey, C. E., Barnes, A. C., and Cruickshank, J. M. (2003) *Proc. Natl. Acad. Sci. U.S.A.* **100,** 4557–4561
48. White, K. L., Margot, N. A., Wrin, T., Petropoulos, C. J., Miller, M. D., and Naeger, L. K. (2002) *Antimicrob. Agents Chemother.* **46,** 3437–3446
49. Sarafianos, S. G., Das, K., Clark, A. D., Jr., Ding, J., Boyer, P. L., Hughes, S. H., and Arnold, E. (1999) *Proc. Natl. Acad. Sci. U.S.A.* **96,** 10027–10032
50. Sharma, P. L., Nurpeisov, V., Lee, K., Skaggs, S., Di San Filippo, C. A., and Schinazi, R. F. (2004) *Virology* **321,** 222–234
51. Meyer, P. R., Matsuura, S. E., Zonarich, D., Chopra, R. R., Pendarvis, E., Bazmi, H. Z., Mellors, J. W., and Scott, W. A. (2003) *J. Virol.* **77,** 6127–6137
52. Marchand, B., and Götte, M. (2003) *J. Biol. Chem.* **278,** 35362–35372
53. Bazmi, H. Z., Hammond, J. L., Cavalcanti, S. C., Chu, C. K., Schinazi, R. F., and Mellors, J. W. (2000) *Antimicrob. Agents Chemother.* **44,** 1783–1788
54. Feng, J. Y., and Anderson, K. S. (1999) *Biochemistry* **38,** 55–63